

# Triangular Bose-Hubbard trimer as a minimal model for a superfluid circuit

Geva Arwas<sup>1</sup>, Amichay Vardi<sup>2</sup>, Doron Cohen<sup>1</sup>

<sup>1</sup>*Department of Physics, Ben-Gurion University of the Negev, Beer-Sheva, Israel*

<sup>1</sup>*Department of Chemistry, Ben-Gurion University of the Negev, Beer-Sheva, Israel*

The triangular Bose-Hubbard trimer is topologically the minimal model for a BEC superfluid circuit. As a dynamical system of two coupled freedoms it has mixed phase-space with chaotic dynamics. We employ a semiclassical perspective to study triangular trimer physics beyond the conventional picture of the superfluid-to-insulator transition. From the analysis of the Peierls-Nabarro energy landscape, we deduce the various regimes in the  $(\Omega, u)$  parameter-space, where  $u$  is the interaction, and  $\Omega$  is the superfluid rotation-velocity. We thus characterize the superfluid-stability and chaoticity of the many-body eigenstates throughout the Hilbert space.

## I. INTRODUCTION

The experimental study of Bose-Einstein Condensates (BECs) allows the realization of ultracold atomic superfluid circuits [1–14] and the incorporation of a laser-induced weak-link (a bosonic Josephson junction) within them [15]. By rotating such a barrier it is possible to induce current [16] and to drive phase-slips between quantized superfluid states of a low dimensional toroidal ring [15]. Such mesoscopic devices open a new arena for detailed study of complex Hamiltonian dynamics.

The hallmark of superfluidity is a stable non-equilibrium steady-state current. If  $N$  bosons in a rotating ring are condensed into a single plane-wave orbital, one obtains a “vortex state” with a quantized current per particle ( $I/N$ ) [17–20]. For non-interacting bosons the lowest vortex-state is also the ground state. It is stable and carries a microscopically small “persistent current”. By contrast, all higher vortex states are unstable. Interactions change the picture dramatically [21]: the Bogolyubov-spectrum of the one-particle excitations of a vortex-state is modified (e.g. by the appearance of phonons), and hence all vortex-states that satisfy the Landau criterion [22–24] become stable. See Fig. 1 for illustration, and Section VI for extra pedagogical details.

The vortex-state of bosons in a ring constitutes one particular example of a coherent (non-fragmented) state. Other coherent-state solutions may correspond, for example, to all bosons condensed in a localized orbital (bright soliton) [17], or in an orbital that has a notch (dark soliton) [18, 19]. From such non-stationary classical solutions one can superpose stationary quantum eigenstates whose angular momentum is not quantized.

The above picture is missing a central ingredient: there is no reference to the global structure of the underlying phase-space that dictates the dynamics. Vortex-states and solitons are minima or maxima of the energy landscape, and the Bogolyubov spectrum merely reflects the linear-stability analysis in the vicinity of these solutions. We are therefore motivated to consider the simplest paradigm for a superfluid circuit which still allows the thorough investigation of its phase-space structure. The natural choice for such a model is bosons in a one-dimensional ring as in Ref. [20] or its discrete  $M$  site ver-

sion, described by the Bose-Hubbard Hamiltonian (BHH) [25–28] as in Ref. [29].

The phase-space of the ring model was studied within a two-orbital approximation [30]. However, such an approximation is not a valid minimal model by itself. From a *topological* point of view the minimal model for a superfluid circuit has to involve  $M=3$  sites: a triangular Bose-Hubbard trimer (this would be equivalent to three non-localized modes). A close relative is the linear Bose-Hubbard trimer. The trimer phase-space has been partially studied in several papers [31–43], and has been

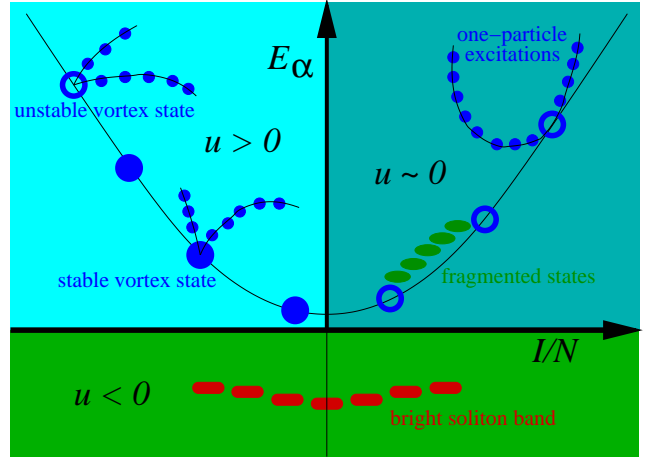


FIG. 1: Representative eigen-energies  $E_\alpha$  of a rotating ring system are classified by the current  $I$  they carry in the rotating frame of reference. The filled and hollow blue circles represent stable and unstable vortex-states for which  $I/N$  is quantized. The blue dots represent their Bogolyubov one-particle excitations. On the upper right  $u$  is vanishingly small, while on the upper left  $u$  is large and positive, resulting in phonon branches. The green elliptic dots represent fragmented states (here the particles are divided between two vortex orbitals). For negative  $u$  (lower plane) there are stable bright soliton solutions. Red oval dots represent eigenstates that are formed by superposition of such solitons. For positive  $u$ , and appropriate rotation frequency, one may observe additional type of eigenstates that are formed of dark solitons (not illustrated). Adding weak disorder, the unstable vortex-states would mix with their excitations, and the soliton band would decompose into a set of standing solitons.

recognized as a building block for studies of transport [44, 45] and mesoscopic thermalization [46, 47].

In this work we study the triangular Bose-Hubbard trimer as a topologically minimal model for a BEC superfluid circuit. In particular, we note that the mixed phase-space aspect of the dynamics has far reaching consequences, producing non-trivial physics that goes beyond the conventional picture of the Mott superfluid-to-insulator transition. Our approach relies on the analysis of the Peierls-Nabarro energy landscape [44, 45, 48, 49], from which we deduce various regimes in the  $(\Omega, u)$  parameter-space of the triangular BHH trimer, where  $u$  is the interaction parameter, and  $\Omega$  is the superfluid rotation-velocity. In each of these regimes we outline the structure of phase-space and the classification of the many-body eigenstates. The criteria for the superfluid stability as opposed to chaoticity are thus determined.

## II. A ROTATING DEVICE

In a typical experimental scenario the potential is translated along the circuit, and can be written as  $V(\theta - \Omega t)$ . For theoretical analysis it is more convenient to transform the Hamiltonian to a rotating frame wherein the potential is time-independent. The rotation is thus formally equivalent to the introduction of a magnetic flux  $\Phi$  through the ring. To relate the flux  $\Phi$  to the rotation velocity  $\Omega$  it is sufficient, without loss of generality, to write the one-particle Hamiltonian as follows:

$$\begin{aligned} \mathcal{H} &= \frac{1}{2mR^2} \left( p_\theta - \frac{\Phi}{2\pi} \right)^2 + V(\theta) & (1) \\ &\equiv \mathcal{H}_0 - \Omega p_\theta + \text{const} & (2) \end{aligned}$$

where  $R$  is the radius of the ring,  $\theta$  is the angular position coordinate, and  $p_\theta$  is the conjugate angular momentum. In the second equality  $\mathcal{H}_0$  is defined as the Hamiltonian in the absence of magnetic flux. Consequently one observes that  $\mathcal{H}$  is formally the same Hamiltonian as that of a rotating system with the implied identification

$$\Omega = \left[ \frac{1}{mR^2} \right] \frac{\Phi}{2\pi}. \quad (3)$$

In references [17–19] units are set such that the pre-factor in the square brackets is unity. Hence, throughout this paper  $\Phi = 2\pi$  corresponds to  $\Omega = 1$  in these references.

We consider  $V(\theta)$  consisting of  $M$  deep wells, for which a tight-binding model is appropriate. The hopping frequency  $K = 1/(m_{\text{eff}}a^2)$  is conventionally expressed in terms of the lattice constant  $a = 2\pi R/M$  and an effective mass  $m_{\text{eff}}$ . The magnetic flux  $\Phi$  implies the vector potential  $A = \Phi/(2\pi R)$ . The phase acquired as particles hop between wells is  $A \times a = \Phi/M$ . For practical purpose the relation between  $\Omega$  and  $\Phi$  can be re-written as

$$\Omega = \frac{2\pi}{M^2} \left( \frac{m_{\text{eff}}}{m} \right) K \Phi \quad (4)$$

Note that both  $K$  and  $\Omega$  have dimensions of frequency.

## III. THE TRIMER HAMILTONIAN

Few-mode Bose-Hubbard systems are experimentally accessible, highly tunable, and theoretically tractable by a wide range of techniques. Since boson number is conserved, their Hilbert spaces are of finite dimension, and yet their classical dynamics is non-integrable. The BHH in a rotating frame is

$$\mathcal{H} = \sum_{j=1}^M \left[ \frac{U}{2} a_j^\dagger a_j^\dagger a_j a_j - \frac{K}{2} \left( e^{i(\Phi/M)} a_{j+1}^\dagger a_j + \text{h.c.} \right) \right] \quad (5)$$

Here  $j \bmod(M)$  labels the sites of the ring,  $a_i$  and  $a_i^\dagger$  are canonical destruction and creation operators in second quantization,  $K$  is the hopping frequency, and  $U$  is the on-site interaction.

As described in the previous section, the phase  $\Phi$  reflects the rotation frequency  $\Omega$  of the ring. Without loss of generality we assume  $\Phi \in [0, \pi]$ , and  $K > 0$ , and  $U > 0$ . Negative  $K$  is the same as positive  $K$  with  $\Phi \mapsto \Phi + \pi$ . Negative  $U$  is the same as positive  $U$  with a flipped energy landscape ( $\mathcal{H} \mapsto -\mathcal{H}$ ). Negative  $\Phi$  is related to positive  $\Phi$  by time reversal.

The Hamiltonian  $\mathcal{H}$  commutes with the total particle number  $\mathcal{N} = \sum_i a_i^\dagger a_i$ , hence the *operator*  $\mathcal{N}$  is a constant of motion, and without loss of generality can be replaced by a definite *number*  $N$ .

In a semi-classical context a bosonic site can be regarded as an harmonic oscillator, and one substitutes  $a_j = \sqrt{\mathbf{n}_j} e^{i\varphi_j}$ . Dropping a constant we get

$$\mathcal{H} = \sum_{j=1}^M \left[ \frac{U}{2} \mathbf{n}_j^2 - K \sqrt{\mathbf{n}_{j+1} \mathbf{n}_j} \cos \left( (\varphi_{j+1} - \varphi_j) - \frac{\Phi}{M} \right) \right] \quad (6)$$

Since  $N$  is a constant of motion Eq.(6) describes  $M-1$  coupled degrees of freedoms. Accordingly the trimer ( $M=3$ ) is equivalent to two coupled pendula, featuring mixed-phase space with chaotic dynamics. In practice it is convenient to define phase-space configuration coordinates  $r = (r_1, r_2)$  and associate variables  $q = (q_1, q_2)$  as follows:

$$\begin{aligned} r_1 &= -\frac{1}{2N} (\mathbf{n}_3 - \mathbf{n}_2) & r_2 &= -\frac{1}{2N} (\mathbf{n}_1 - \mathbf{n}_3) & (7) \\ q_1 &= \varphi_3 - \varphi_2 & q_2 &= \varphi_1 - \varphi_3 & (8) \end{aligned}$$

Note that in a *semi-classical* perspective  $r$  and  $q$  are canonically conjugate variables with commutation relation  $[r, q] = i\hbar$ , where  $\hbar = 1/N$ .

Given the model parameter  $(\Phi, K, U, N)$  we use standard re-scaling procedure (of  $\mathbf{n}$  as described above, and of time) in order to deduce that the classical equation of motion are controlled by two dimensionless parameters  $(\Phi, u)$ , while upon quantization we have the third dimensionless parameter  $\hbar = 1/N$ . The dimensionless interaction strength is

$$u = \frac{NU}{K}. \quad (9)$$

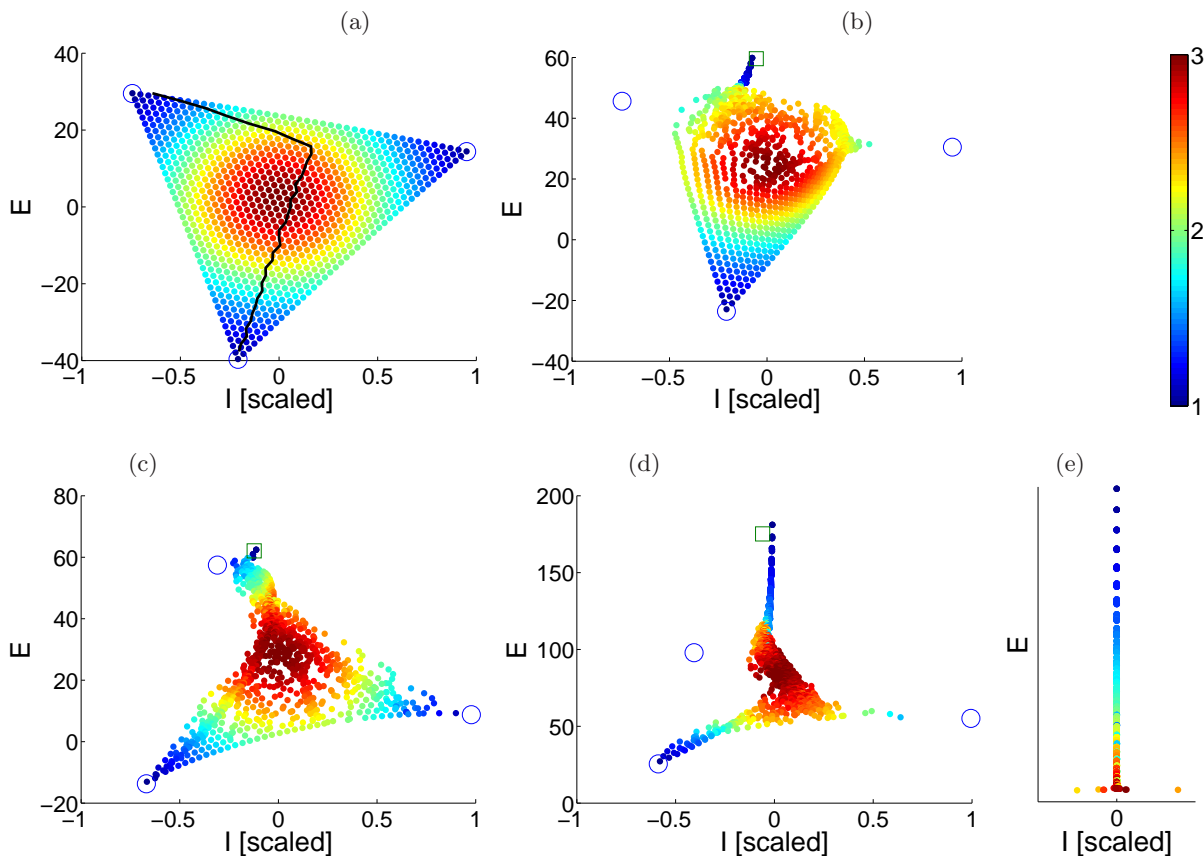


FIG. 2: The quantum spectrum of  $N = 42$  bosons in a triangular BEC trimer. Panels (a-e) are for  $(\Phi, u)$  as follows:  $(0.2\pi, 0.2)$ ;  $(0.2\pi, 2.5)$ ;  $(0.7\pi, 2.5)$ ;  $(0.6\pi, 8.5)$ ;  $(0.6\pi, 1470)$ . Each point represents an eigenstate color-coded by its purity (blue  $(1/S) \sim 1$  to red  $(1/S) \sim 3$ ), and positioned according to its energy and its current. For negligible interactions vortex-states become exact eigenstates, represented as empty blue circles. In panels (b-d), due to bifurcations, stable solitons are found in the expected semi-classical locations (indicated by empty green squares). In (c) as opposed to (b) the rotation frequency is large enough to stabilize an intermediate vortex-state. In (e) as opposed to (d) the interaction is strong, and the Mott transition of the ground state is reflected in its low purity. The remaining low-purity fragmented states dwell in the chaotic sea and do not carry a quantized current. For large  $M$  we expect their dispersion in  $I$  to shrink further down compared with the quantized values. The thick black line in (a) is the microcanonical value of  $I$ .

In view of the optional continuum limit it is natural to define classical and quantum versions of  $u$  as follows:

$$u^{cl} = \frac{2}{M}u \quad (10)$$

$$u^{qm} = \frac{Mu}{N^2} \quad (11)$$

The use of  $u^{cl}$  is preferable over  $u$  for systems with  $M \gg 1$  sites. For the trimer ( $M = 3$ ) we shall use the bare  $u$  throughout the numerical presentation.

#### IV. THE CURRENT

The eigenstates  $|E_\alpha\rangle$  of Eq. (5) are characterized by the current  $I = \langle \mathcal{I} \rangle$  that they carry. The outcome of the standard definition  $\mathcal{I} \equiv -(\partial\mathcal{H}/\partial\Phi)$  is gauge dependent. For the translation-symmetric gauge of Eq. (5) we get the bond-averaged current. The quantized values of the

current in the case of a vortex-state are

$$I_m = \frac{N}{M}K \sin\left(\frac{1}{M}(2\pi m - \Phi)\right) \quad (12)$$

where  $m$  is an integer. For one particle in a ring both  $\mathcal{H}$  and  $\mathcal{I}$  commute with the non-degenerate displacement operator  $\mathcal{D}$ , and hence commute with each other. This is no longer true for  $N$  particles where due to the interactions *the current is not a constant of motion*. By contrast, the displacement operator still commutes with  $\mathcal{H}$  but decomposes it merely into  $M$  blocks. Thus, unlike in a continuous ring system, the current  $\mathcal{I}$  can not be identified with the total angular momentum.

In a classical context the average current of a microcanonical ergodic state can be calculated using the standard statistical-mechanics prescription:

$$I_E = \frac{1}{\mathcal{A}} \int \mathcal{I}(r, q) \delta(\mathcal{H}(r, q) - E) d\vec{r}d\vec{q} \quad (13)$$

where the normalization  $A$  is the area of the energy surface: the same integral but without  $\mathcal{I}$  in the integrand.

If the system were fully chaotic with microcanonical-like quantum eigenstates spread throughout the energy surfaces,  $I$  would have been a well-defined function of  $E$  with very small fluctuations. In Fig.2 we display the numerically calculated spectrum of the BHH Eq.(5). Each eigenstate is represented by a point  $(E_\alpha, I_\alpha)$ , where

$$I_\alpha = \langle \mathcal{I} \rangle_\alpha, \quad \alpha = \text{eigenstate} \quad (14)$$

We observe that there is very large dispersion of  $I_\alpha$  values around the microcanonical  $I_E$  value. This is due to having a mixed phase-space, and is further affected by quantum interference - both issues will be addressed in the following sections. Few representative examples of eigenstates are shown in Fig.3. For each eigenstate  $|E_\alpha\rangle$  we plot the probability density in  $r$  space:

$$|\Psi(r)|^2 = \left| \langle r | E_\alpha \rangle \right|^2. \quad (15)$$

The image axes are  $\mathbf{n}_1 - \mathbf{n}_2$  and  $\mathbf{n}_3$ . The classification of the eigenstates will be discussed in the following sections.

## V. CONDENSATION AND PURITY

The purpose of this section is to define what is a *condensate*; and to clarify that it can be regarded as a *coherent-state* which is supported by a *fixed-point* of the underlying classical Hamiltonian. In particular we distinguish between *vortex-states* and *solitons*.

A non-fragmented condensate is formed by macroscopic occupation of a single one-particle orbital  $k$ . Namely it can be written as  $(b_k^\dagger)^N |vacuum\rangle$ , where  $b_k^\dagger = \sum_j \alpha_j^k a_j$  creates a particle in some superposition of the site modes, with  $c$ -number coefficients  $\alpha_j^k$ . Such state can be regarded as a many-body coherent state in the generalized sense of Perelomov [50]. Optionally it can be pictured as a minimal wave-packet that is situated at some point  $z = (r, q)$  of phase-space.

In order to characterize quantitatively the fragmentation of an eigenstate it is natural to define the following purity measure

$$S \equiv \text{trace}(\rho^2) \quad (16)$$

where  $\rho_{ij} = \langle a_j^\dagger a_i \rangle$  is the one-body reduced probability matrix. Roughly speaking  $1/S$  corresponds to the number of orbitals occupied by the bosons. The value  $S = 1$  indicates a coherent-state, while a low value indicates that the condensate is fragmented into several orbitals.

We would like to clarify why some eigenstates of the Hamiltonian resemble coherent states. For this purpose recall that the quantum eigenstates of the Hamiltonian are semi-classically supported by the energy surfaces  $\mathcal{H}(r, q) = E$ . If the energy surface is fully connected and chaotic one expects the  $E_\alpha \sim E$  eigenstates to be ergodic,

microcanonical-like. A stable fixed-point of the Hamiltonian can be regarded as a zero volume energy surface. In its vicinity the dynamics looks like that of harmonic oscillation. Accordingly a Planck-cell volume at that region can support a coherent-state. In the BHH context the Planck-cell volume is determined by  $1/N$ .

Our Hamiltonian always has at least two fixed-points: one that corresponds to the lowest energy, and one that corresponds to the upper-most energy. Accordingly both the ground-state and the upper-state are ‘‘coherent states’’ in the large  $N$  limit. Note that the upper-state can be regarded as the ground-state of  $-\mathcal{H}$ . The intermediate energy surfaces have a large area, hence microcanonical-like states that are located there are not ‘‘coherent’’. But if we have mixed-phase space we might find fixed-points at intermediate energies. Such fixed-points might support meta-stable coherent states.

Vortex-states are eigenstates that *resemble* a condensate in one of the single-particle momentum-orbitals of the ring. They are supported by fixed-points that are aligned along the  $r = 0$  axis of phase-space, with  $q = (2\pi/M)m$ . Vortex-states as well as their one-particle excitations have high purity  $S \sim 1$ .

Self-trapped states, also known as bright solitons, are eigenstates that *resemble* a condensate in a localized orbital. They are supported by fixed-points that are generated via a bifurcation once a vortex-state loses its stability. This bifurcation scenario will be analysed in Section IX.

## VI. THE ENERGY SPECTRUM

Representative illustrations of the  $E_\alpha$  spectrum are presented in Fig.2. Eigenstates are classified by their *current* ( $I$ ), and colour-coded according to their *one-particle purity* ( $S$ ). In Fig.3 we display representative examples of eigenstates: the ground state vortex; a metastable vortex; a self trapped bright soliton; and a low purity state in the chaotic sea.

Comparing Fig.2 with Fig.1, we observe that: **(a)** The ground state is vortex-state carrying the expected quantized current. It retains its purity up to an extremely large value of  $u \sim N^2$  where the transition to a Mott insulator takes place (see ‘Mott transition’ section). **(b)** For small  $u$ , there is a stable vortex-state at the top of the energy landscape. **(c)** If  $u$  is large enough, the upper vortex-state bifurcates and is replaced by 3 self-trapped solitons carrying very little current (see ‘self trapping’ section). **(d)** It is feasible to have an additional high purity vortex-state in an intermediate energy range (see ‘metastability’ section). **(e)** The majority states are highly fragmented and are not characterized by a well-defined quantized value of current.

Below we provide a semi-classical interpretation of the above findings, and deduce a schematic diagram of the  $(\Phi, u)$  regimes.

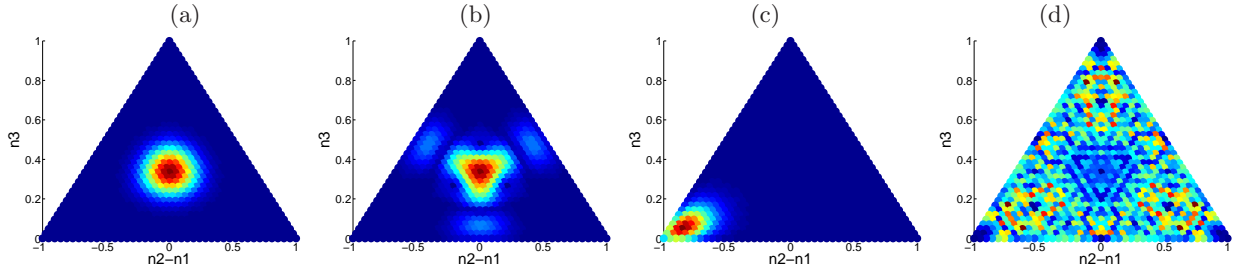


FIG. 3: Representative eigenstates for the spectrum that is plotted in panel (c) of Fig. 2. Each panel is an image of the probability density in  $r$  space, where blue and red correspond to zero and maximum density respectively. (a) The ground state vortex  $E_\alpha \approx -14$ . (b) A metastable vortex  $E_\alpha \approx 9$ . (c) A self trapped bright soliton  $E_\alpha \approx 62$ . (d) A low purity state in the chaotic sea  $E_\alpha \approx 29$ . The color code is blue (low density) to red (high density).

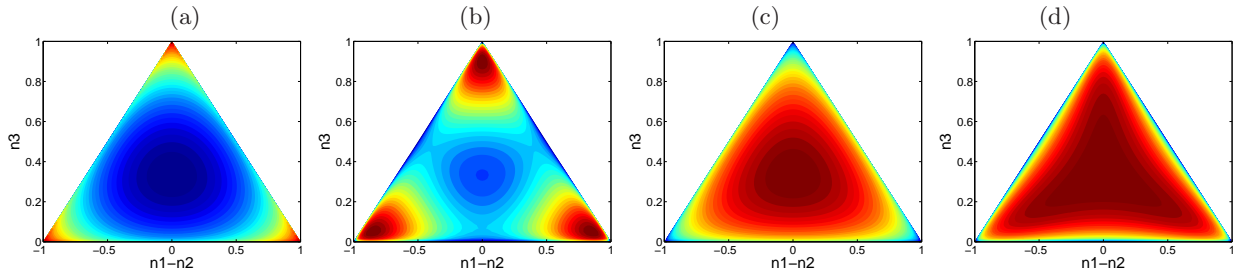


FIG. 4: Images of the energy surfaces  $V_m(r)$ . (a) and (b) are the lower and the upper energy surface for  $(\Phi, u) = (\pi/4, 2)$ , illustrating regime (d) in Fig. 6. (c) and (d) are the upper energy surfaces for  $(0.8\pi, 0.4)$  and  $(0.8\pi, 1.8)$ , illustrating regimes (a) and (b) in Fig. 6. The color code is blue (low energy) to red (high energy). See Fig. 5 for a section along the symmetry line.

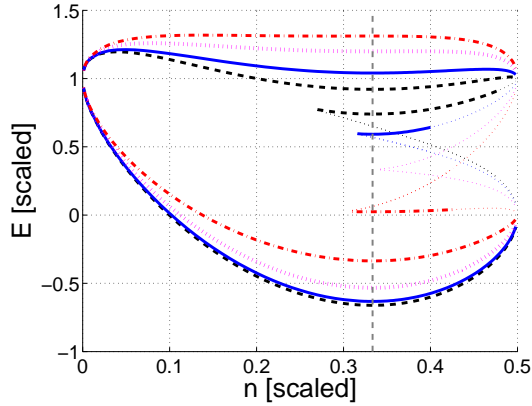


FIG. 5: A section along the symmetry line  $n_1 = n_2 = n$ , for  $u = 2$  and  $\Phi = \pi/4$  (solid line), as well as for  $\Phi = 0.1\pi$  (dashed), and  $0.5\pi$  (dotted), and  $0.8\pi$  (dashdot). Each section shows the upper surface and also the lower and intermediate surfaces, which are formed of extremal points. The thin dotted segments are formed of saddle points. As  $\Phi$  becomes larger the intermediate surface  $V_-(r)$  goes down in energy. For  $\Phi < \pi/2$  it is formed of maxima, and its area shrinks to zero as  $\Phi$  is increased. For  $\Phi > \pi/2$  it becomes a surface of minima, and its area expands back.

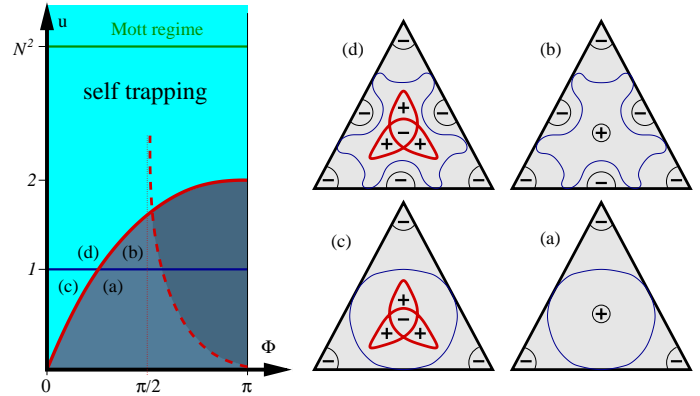


FIG. 6: Regime diagram of the triangular BEC trimer. The model parameters are  $(\Phi, u)$ . The thick solid lines divide the diagram into four quarters (a-d). In each quarter the topography of the upper energy surface is different, as schematically illustrated on the right. The thick dashed line indicates the classical stability threshold of the intermediate energy surface. In the quantum analysis we observe quasi-stability as  $\Phi = \pi/2$  is crossed: see the text for details and Fig. 8 for demonstration.

## VII. STABILITY ANALYSIS

The BHH formally describes a set of coupled oscillators. Schematically we can write the Hamiltonian as  $H(z)$  with  $z = (r, q)$  and  $\hbar = 1/N$ . This Hamiltonian has  $M-1$  freedoms. A stable fixed-point  $z_0$  can support a coherent-state provided  $\hbar$  is small enough.

At  $r = 0$  we always have 3 fixed-points that correspond quantum-mechanically to condensation in one of the 3 momentum orbitals of the trimer. The questions are: (i) whether these fixed-points are stable; (ii) whether they can support a coherent quantum state. In this section we discuss the first question. In Section X (Mott transition) and in Section XI (Metastability) we discuss the second question, which is related to having a finite  $\hbar$ .

Fixed-point stability is determined by linearization of the Hamiltonian in its vicinity, resulting in a set of Bogoliubov de-Gennes (BdG) equations. This set gives  $M-1$  frequencies  $\omega_k$  for the Bogoliubov excitations. Frequencies of different signs imply *thermodynamic* instability, as occur in Hamiltonian of the type  $H = \omega_1 n_1 + \omega_2 n_2$  with  $\omega_1 > 0$  and  $\omega_2 < 0$ . Complex frequencies indicate *dynamical* instability (hyperbolic fixed-point), as occur in Hamiltonian  $H = p^2 - x^2$ .

Consider a fixed-point that becomes thermodynamically unstable as a result of varying some parameters in the Hamiltonian, or due to added disorder. This means that the island that had surrounded the fixed-point is now opened. In quantum terms one may say that the former vortex-state can mix with the a finite density of zero-energy excitations, leading to a low purity, possibly ergodic set of eigenstates.

In remaining part of this section we clarify how the BdG stability analysis is related to the Landau criterion for the stability of a superfluid motion, and mention the known result for an  $M \gg 1$  ring.

The standard presentation of the Landau criterion takes the liquid as the frame of reference, with the walls moving at some velocity  $\Omega$ . It is then argued that energy cannot be transferred from the walls to the liquid if the excitation energies satisfy  $\omega_k^{(0)} > \Omega k$  for any wavenumber  $k$  of the excitation. In the case of phonons ( $\omega_k^{(0)} = ck$ ) this implies that  $\Omega$  should be smaller than the speed of sound  $c$ .

It is conceptually illuminating to write the Landau criterion in the reference frame where the walls are at rest, and the Hamiltonian becomes time independent. In this frame the superfluid is rotating with frequency  $\Omega_m = -\Omega$ . The Landau conditions takes the form  $\omega_k > 0$  for any  $k$ , where

$$\omega_k = \omega_k^{(0)} + \Omega_m k, \quad [\text{standing device}] \quad (17)$$

are the excitation energies of the vortex-state. For an  $M \gg 1$  ring, taking the continuum limit, the Landau criterion reasoning implies that the excitation energies of the  $m$ th vortex-state in a rotating device are

$$\omega_k = \sqrt{(\epsilon_k + \tilde{u})\epsilon_k} - (\Omega - \Omega_m)k \quad (18)$$

where  $\Omega = \Phi/(2\pi)$  is the scaled rotation frequency of the device, and  $\Omega_m = m$  is the quantized rotation frequency of the superfluid. The integer  $k$  is the wavenumber of the Bogoliubov excitation, while  $\epsilon_k = (1/2)k^2$  is the unperturbed single-particle energy, and  $\tilde{u}$  is the appropriately scaled interaction. Note that the first term has the form  $ck$  for small  $k$ , where the sound velocity is  $c = \sqrt{\tilde{u}/2}$ . The implications of this expression on the stability of the vortex-states is illustrated in Fig.1.

It should be clear that the Landau criterion is not applicable in the case of a finite  $M$  system, because we cannot use Galilean transformation to relate  $\omega_k$  to  $\omega_k^{(0)}$ . Therefore we have to utilize the phase-space picture of the dynamics in order to determine the regime diagram of the rotating trimer. Whenever a vortex-state loses its stability, irrespective of the nature of the Bogolyubov excitations, we understand that superfluidity is lost.

The “standing walls” formulation of the Landau-criterion makes transparent the connection to the Fermi-golden-rule picture (FGRP) and to the semi-classical picture (SCP). In the FGRP the walls, or optionally some weak disordered potential, induces first-order coupling of the vortex-state to its Bogolyubov one-particle excitations. Accordingly, in the FGRP language the Landau condition is phrased as the requirement of not having Bogolyubov excitations with the same energy as the vortex-state. In the SCP one considers, instead of “weak disorder”, a weak perturbation of the vortex-state. The linear-stability analysis tells us whether the vortex-state is stable or not, leading again to the Landau criterion.

If the vortex-state is meta-stable, then quantum tunnelling or thermal activation are required in order to get a “phase slip” to a lower vortex-state. This goes beyond the “Landau criterion”, but still can be addressed using the SCP, possibly combined with FGRP and optionally using WKB-type approximation.

## VIII. THE REGIMES DIAGRAM

We regard  $r$  as a triangular configuration space. It consists of points  $(\mathbf{n}_1, \mathbf{n}_2, \mathbf{n}_3)$ , such that  $\mathbf{n}_1 + \mathbf{n}_2 + \mathbf{n}_3 = N$ . The phase differences  $q$  are regarded as the conjugate momenta: they determine the velocity  $\dot{r}$ . The energy landscape of the Hamiltonian can be visualized using the Peierls-Nabarro surfaces  $V_m(r)$ , formed of its extremal points under phase variation [44, 45, 48, 49]. Lower Peierls-Nabarro surfaces are thus defined as

$$V(r) \equiv \min_{\varphi} [\mathcal{H}(r, \varphi)] \quad (19)$$

whereas upper Peierls-Nabarro surfaces are defined with  $\max[\dots]$  instead of  $\min[\dots]$ . Additionally we may have pieces of surfaces that consists of saddle points.

In our model we have three surfaces: a lower surface  $V_0(r)$ , an intermediate surface  $V_-(r)$ , and an upper surface  $V_+(r)$ , as shown in Fig.4 (images) and in Fig.5 (sections). For  $\Phi < \pi/2$  the intermediate surface is an “upper” surface that is formed of local maxima, whereas for

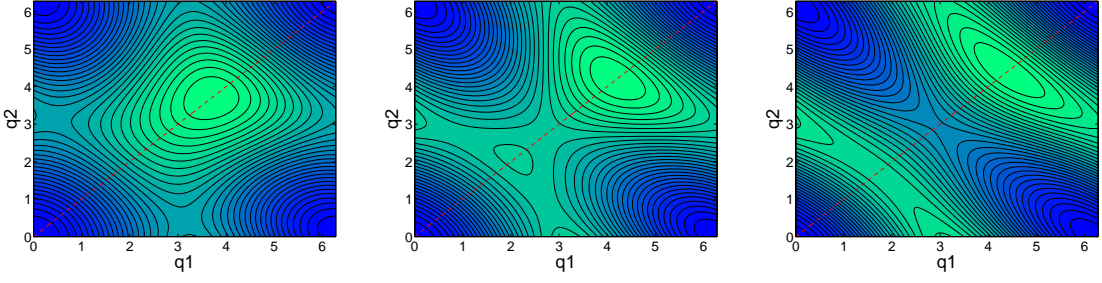


FIG. 7: Images of  $E = \mathcal{H}(r, \varphi)$  as a function of  $q_1$  and  $q_2$  for  $\Phi = 0.2\pi$ . In the three panels  $n_1 = n_2 = n$ , hence the fixed-points of interest are along the symmetry line  $q_1 = q_2$ . The left panel is at  $n = (1/10)N$ , and it has a single minimum and a single maximum. The middle panel is at the symmetry point  $r_0 = 0$ , where  $n = (1/3)N$ , and it has a single minimum and two maxima. Consequently in the vicinity of  $r_0$  we have three energy surfaces. The right panel is at  $n = (9/20)N$ , and it has again a single minimum and a single maximum.

$\Phi > \pi/2$  it is a “lower” surface. It should be clear that a stable fixed-point is either a minimum of a “lower” surface or a maximum of an “upper” surface. Note also that the upper-most fixed-point can be envisioned as the ground-state of the  $U \mapsto -U$  Hamiltonian.

The diagram of Fig.6 summarizes the different parametric regimes of the model: each regime is characterized by a different type of  $V_m(r)$  topography. The central point  $r_0 = 0$  is a fixed-point of the 3 surfaces, with energies  $E_m = V_m(r_0)$ . The fixed point  $E_0$  is always stable. In contrast, the  $E_{\pm}$  fixed-points may be stable or unstable, depending on their curvature  $V_{\pm}''(r_0)$ , where prime denotes differentiation in the “radial” direction.

The fixed-points are situated on the symmetry lines in  $r$  space. So we can restrict the analysis along, say,  $\mathbf{n}_1 = \mathbf{n}_2 = n$ , hence  $\mathbf{n}_3 = N - 2n$ , and

$$\begin{aligned} \mathcal{H}(r, q) = & \frac{U}{2} (\mathbf{n}_1^2 + \mathbf{n}_2^2 + \mathbf{n}_3^2) \\ & - K \left( \sqrt{\mathbf{n}_2 \mathbf{n}_3} \cos(q_1 - \frac{\Phi}{3}) + \sqrt{\mathbf{n}_3 \mathbf{n}_1} \cos(q_2 - \frac{\Phi}{3}) \right. \\ & \left. + \sqrt{\mathbf{n}_1 \mathbf{n}_2} \cos(q_1 + q_2 + \frac{\Phi}{3}) \right) \end{aligned} \quad (20)$$

The lowest surface ( $m = 0$ ) has a trivial topography. In particular for  $\Phi = 0$  the lower surface is

$$\begin{aligned} V_0(r) = & \frac{U}{2} (\mathbf{n}_1^2 + \mathbf{n}_2^2 + \mathbf{n}_3^2) \\ & - K (\sqrt{\mathbf{n}_2 \mathbf{n}_3} + \sqrt{\mathbf{n}_3 \mathbf{n}_1} + \sqrt{\mathbf{n}_1 \mathbf{n}_2}) \end{aligned} \quad (21)$$

For general  $\Phi$  the extremal values (at a given  $r$  location) are still situated along the line  $q_1 = q_2$ . Depending on  $\mathbf{n}$  and  $\Phi$  we have either a single minimum and a single maximum, or two minima and a maximum, or a minimum and two maxima, see Fig.7. It follows that one has to find the 3 extremal points  $q_m(n)$  of the function

$$\begin{aligned} H(q; n) = & \frac{1}{6} N^2 U + 3U \left( n - \frac{N}{3} \right)^2 \\ & - K \left( 2\sqrt{(N - 2n)n} \cos(q - \frac{\Phi}{3}) + n \cos(2q + \frac{\Phi}{3}) \right) \end{aligned} \quad (22)$$

Then one obtains a section of the surface  $V_m(r)$  along the principal “radial” direction  $\mathbf{n} = (n, n, N - 2n)$

$$V_m(n) = H(q_m(n); n) \quad (23)$$

The most interesting fixed-points of  $V_m(r)$  are situated at the central point  $\mathbf{n} = (N/3, N/3, N/3)$ , for which  $n = N/3$ . The three  $r_0$  fixed-points support the vortex-states. The energies of the fixed-points are:

$$E_m = V_m(r_0) = \frac{1}{6} N^2 U - NK \cos\left(\frac{2\pi m - \Phi}{3}\right) \quad (24)$$

with  $m = 0, \pm 1$ . Note that  $I_m = -dE_m/d\Phi$ . A lengthy but straightforward calculation leads to the following result for the curvature at  $r_0$ . This is required in order to determine whether they are stable or not:

$$\begin{aligned} V_{\pm}''(r_0) = & \frac{d^2 H(q_{\pm}(n), n)}{dn^2} \Big|_{N/3} \\ = & 6 \frac{K}{N} \left[ u - \frac{6 - 9 \cos\left(\frac{\pi \pm 2\Phi}{3}\right) - 3 \cos\left(\frac{\pi \mp 4\Phi}{3}\right)}{6 \cos\left(\frac{\pi \mp \Phi}{3}\right) - 2 \cos(\Phi)} \right] \end{aligned} \quad (25)$$

We shall use this result in the subsequent discussion of self-trapping and meta-stability.

## IX. SELF TRAPPING

For the  $M=2$  dimer, when  $u < 1$  the energy landscape stretches between a minimum that corresponds to condensation in the lower orbital, and a maximum that corresponds to condensation in the upper orbital. For  $u > 1$  the maximum bifurcates and accordingly there are two elliptic islands of self-trapped motion. Going back to the trimer, one realizes that the dimer type bifurcation at  $u = 1$  takes place along the edges of the upper energy surface  $V_+(r)$ . But if  $u > 1$  the two maxima that are located on each edge are merely the corners of the central ‘hump’ (see Fig.6bd). Hence  $u = 1$  is not the threshold for self-trapping.

Self-trapping in the trimer is related to the stability of the  $r_0$  fixed-point in the upper energy surface. If  $V_+''(r_0) > 0$  this upper vortex-state bifurcates into 3 maxima that support “self-trapped” states, also known as bright solitons. The self-trapping transition is reflected in the current dependence as demonstrated in Fig. 8. Namely, the current in panel (a) becomes very small once the classical stability border (sashed curve) is crossed. In panel (b) we confirm that the loss of stability is reflected by loss of purity: once the  $r_0$  fixed-point loses stability the vortex-state is replaced by 3 soliton-band-states that stretch over the 3 fixed-point.

In Fig. 8c we repeat the calculation as in Fig. 8b, but with added weak disorder. Namely we add small on-site energy shifts to the Hamiltonian Eq.(5) in order to break the translational invariance of the system. These added random shifts are much smaller than the inter-site hopping  $K$ . They do not affect the stability of the vortex states but they prevent the formation of a soliton band. Note that for  $M \gg 1$  the soliton band would be exponentially narrow. Due to the added weak disorder the soliton-band states disintegrate into self-trapped coherent states that have high purity. In fact some self-trapping also happens in the numerics of panel (b) due to the finite accuracy of the computer.

The above bifurcation scenario appears contradictory to common wisdom. For an  $M$  site ring self-trapping is anticipated when the self-induced potential is deeper than the binding energy, leading to the condition  $u^{cl} > 1$ . Contrary to this naive expectation, Eq.(25) for the trimer implies that the threshold for self-localization is vanishingly small at the limit  $\Phi \rightarrow 0$ . The explanation for this anomaly is as follows: for  $\Phi = 0$  the  $m = \pm 1$  angular-momentum orbitals are degenerate, hence any small  $U$  results in 3 maxima in  $V_+(r)$ . In the case of an  $M$  site ring any small  $U$  results in  $M$  maxima. But if  $M \gg 1$  these maxima represent states that have very weak modulation in the site occupation rather than self-trapping.

## X. MOTT TRANSITION

The BEC ground state corresponds to the minimum of the lower  $V(r)$  surface, which is an elliptic island. If  $u$  is too large this island becomes too small to support a coherent-state and the ground state number-squeezes towards a Fock-basis state. For a Bose-Hubbard dimer ( $M=2$ ) the ground-state becomes a fragmented Fock-state of 50% – 50% site occupation if  $u > N^2$ . See e.g. [51]. More generally, for an  $M$  site ring, the Mott superfluid-insulator transition is controlled by the *quantum* dimensionless parameter  $u^{qm}$  of Eq.(10). As  $u^{qm} > 1$  the ground state loses its one-body coherence and approaches a Fock-state of equal site occupation.

It is important to emphasize that in the semi-classical perspective  $1/N$  plays the role of  $\hbar$ . The “classical” regimes in Fig. 6 are related to the topology of phase-space: they can be resolved if  $\hbar$  is sufficient small, but

do not depend on  $\hbar$ . In contrast, the “quantum” Mott transition has to do with having a finite  $\hbar$ . Due to having a finite Planck-cell the lower surface of the Hamiltonian cannot support a coherent-state. Instead one observes, see e.g. Fig. 2e, a glassy set of low energy fragmented Fock-states. The glassiness is due to the possibility to play with the occupation whenever  $N/M$  is not an integer, or due to having some on-site disorder. The Mott transition becomes “sharp” only in the thermodynamic limit of having large  $M$ , keeping  $N/M$  constant.

## XI. METASTABILITY

Having examined the minimum of the lowest Peierls-Nabarro surface  $V_0(r)$  that undergoes a Mott transition, and the maximum of upper surface  $V_+(r)$  in connection with self-trapping, we turn our attention to the intermediate surface  $V_-(r)$ . We observe in Fig. 2 that a dynamically (meta)stable vortex-states can be found in the middle of the energy spectrum. The  $\Phi$  threshold for stabilization is deduced from the condition  $V_-''(r_0) > 0$  provided  $V_-(r)$  is a “lower” surface. This border is illustrated schematically in Fig. 6 and analytically in Fig. 8 (dashed black line). Unlike self-trapping, here this (classical) border is barely reflected in the numerical results. One observes that large current that is supported by high purity vortex-state appear well beyond the expected stability region. Thus a coherent-solution can be quantum-mechanically stabilized in a flat landscape by interference. We refer to this as “quasi-stability”.

What we call quasi-stability is the possibility to have a quantum coherent eigenstate that is supported by an unstable fixed-point. If we have an *hyperbolic* fixed-point that is immersed in a chaotic sea this is known as “quantum scarring”. Another well known example for quasi-stability is the Anderson strong-localization effect.

Let us point out two examples for quasi-stability in the BHH context. The simplest example is apparently the condensation of bosons in the upper orbital of a dimer[52]: this is formally the same as saying that the upper position of a pendulum is quasi-stable rather than unstable. An additional example is encountered in the case of a kicked dimer [53], which is a manifestation of quantum scarring [54, 55]. In both examples the quasi-stability is related to the low participation number (PN). The PN characterizes a coherent-state that is situated on the hyperbolic point; it estimates how many eigenstates appear in its spectral decomposition. In the first example the deterioration of the purity is small because  $\text{PN} \sim \log(N)$  rather than  $\text{PN} \sim \sqrt{N}$ , while in the second example  $\text{PN} \sim N$  with a prefactor that depends on the Lyapunov exponent.

In the present analysis the traditional paradigms for quantum quasi-stability do not apply. We dare to say that a theory for a new paradigm is required.

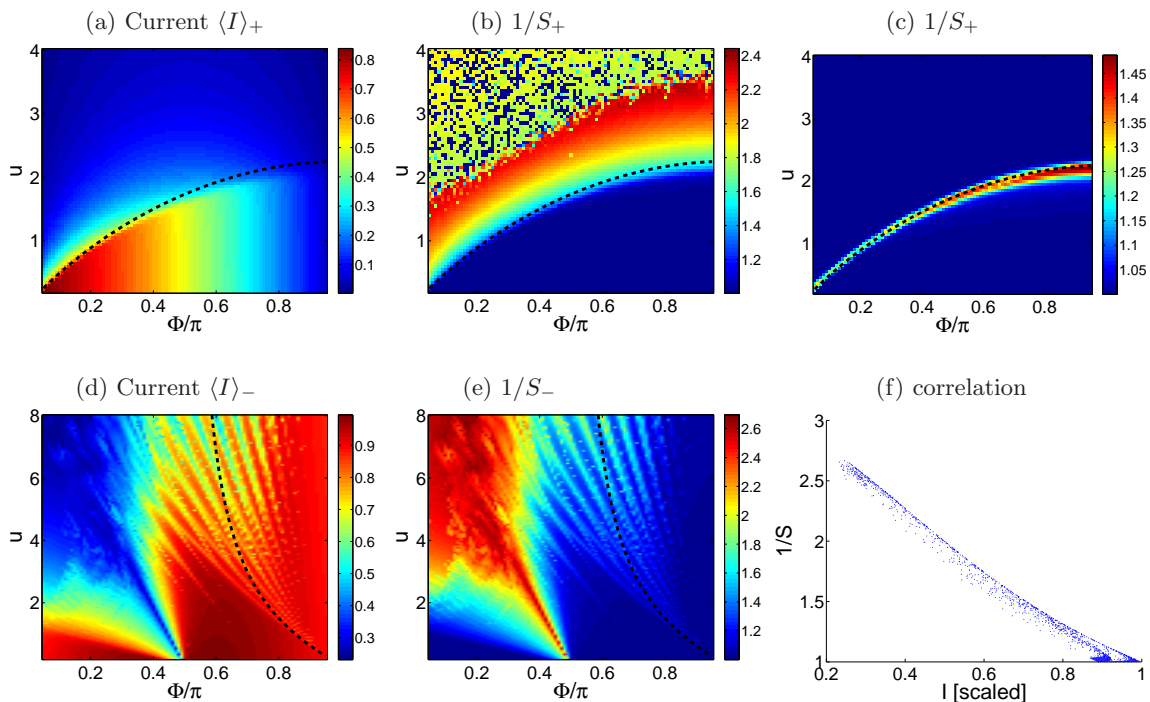


FIG. 8: We consider a trimer with  $N = 42$  bosons. In (a) The current of the upper-energy state is imaged as a function of  $(\Phi, u)$ . It becomes vanishingly small once the self-trapping border (dashed line) is crossed. In (b) we plot the  $1/S$  of the same state, while in (c) we repeat the calculation after adding some weak disorder (see text). Panels (d) and (e) are the same as (a) and (b) but for the intermediate state that has the maximal current. This is a metastable vortex-state if  $S \sim 1$ . Note that the classical stability border (dashed line) fails to provide a valid prediction for loss of purity, which is strongly correlated with low  $I$  values as demonstrated in panel (f).

## XII. CONCLUDING REMARKS

We presented a comprehensive overview of a minimal model for a superfluid circuit. Contrary to the conventional picture we observe that self-trapping can occur for arbitrarily small interaction, and that unstable vortex-states can become quasi-stable. These anomalies reflect the mesoscopic nature of the device: effects that are related to orbital-degeneracy and quantum-scarring cannot be neglected.

A two orbital approximation as in [30] does not qualify as a minimal model for a superfluid circuit, but it captures one essential ingredient: as a parameter is varied a fixed-point can undergo a bifurcation. Specifically a vortex-state can bifurcate into solitons. In the absence of symmetry breaking the bifurcations is into  $M$  solitons, as illustrated in Fig.2 in going from regime (a) to regime (c). These solitons form a band unless the displacement symmetry is broken, say by disorder. The 2 orbital approximation assumes such symmetry breaking, and provides a simplified local description of the bifurcation. A global description of phase-space topology requires to go beyond the 2 orbital approximation. Then one encounters eigenstates that dwell in the chaotic sea. Consequently one can regard the trimer as a bridge towards the classical and the thermodynamic limits. All the required ingredients are here: the topology and the underlying mixed

phase-space.

We note that in a former work [56] it has been argued that for  $\Omega = 0$  metastable vortex-states would be found provided  $M > 4$ . The argument explicitly assumes  $\Omega = 0$ , and it is based on a semiclassical (mean field) stability analysis. We find that for  $\Omega \neq 0$  the semiclassical stability analysis allows metastable vortex-states for  $M = 3$  as well. The results of our semiclassical analysis are summarized by the  $(\Omega, u)$  regime diagram of Fig.6.

But when we go to the quantum analysis we find that the physical picture is further modified quite dramatically due to the manifestation of quantum interference effect that is not expected on the basis of a mean-field theory. This unexpected quasi-stability is effective enough to stabilize metastable vortex-states even if the device is non-rotating!

**Acknowledgments.**— We thank James Anglin, Tony Leggett, and Parag Ghosh for useful communication regarding the observation that for  $\Omega = 0$  metastable vortex-states would be found provided  $M > 4$ . We thank Igor Tikhonenkov and Christine Khripkov for sharing numerical codes that had been used in [47]. This research was supported by the Israel Science Foundation (grant Nos. 29/11 and 346/11) and by the US-Israel Binational Science Foundation (grant No. 2008141).

- 
- [1] C. Raman, M. Kohl, R. Onofrio, D.S. Durfee, C.E. Kulewicz, Z. Hadzibabic, W. Ketterle, Phys. Rev. Lett. **83**, 2502 (1999).
- [2] R. Onofrio, C. Raman, J.M. Vogels, J.R. Abo-Shaeer, A.P. Chikkatur, W. Ketterle, Phys. Rev. Lett. **85**, 2228 (2000).
- [3] S. Inouye, S. Gupta, T. Rosenband, A.P. Chikkatur, A. Gorlitz, T.L. Gustavson, A.E. Leanhardt, D.E. Pritchard, W. Ketterle, Phys. Rev. Lett. **87**, 080402 (2001).
- [4] M. Albiez, R. Gati, J. Folling, S. Hunsmann, M. Cristiani, M.K. Oberthaler, Phys. Rev. Lett. **95**, 010402 (2005).
- [5] P. Engels and C. Atherton, Phys. Rev. Lett. **99**, 160405 (2007).
- [6] D.E. Miller, J.K. Chin, C.A. Stan, Y. Liu, W. Setiawan, C. Sanner, W. Ketterle, Phys. Rev. Lett. **99**, 070402 (2007).
- [7] S. Levy, E. Lahoud, I. Shomroni, J. Steinhauer, Nature (London) **449**, 579 (2007).
- [8] C. Ryu, M.F. Andersen, P. Clade, V. Natarajan, K. Helmerson, W.D. Phillips, Phys. Rev. Lett. **99**, 260401 (2007).
- [9] D. McKay, M. White, M. Pasienski, B. DeMarco, Nature **453**, 76 (2008).
- [10] T.W. Neely, E.C. Samson, A.S. Bradley, M.J. Davis, B.P. Anderson, Phys. Rev. Lett. **104**, 160401 (2010).
- [11] L.J. LeBlanc, A.B. Bardon, J. McKeever, M.H.T. Extavour, D. Jervis, J.H. Thywissen, F. Piazza, A. Smerzi, Phys. Rev. Lett. **106**, 025302 (2011).
- [12] R. Desbuquois, L. Chomaz, T. Yefsah, J. Leonard, J. Beugnon, C. Weitenberg, and J. Dalibard, Nat. Phys. **8**, 645 (2012).
- [13] S. Moulder, S. Beattie, R. P. Smith, N. Tammuz, Z. Hadzibabic, Phys. Rev. A **86**, 013629 (2012).
- [14] A. Ramanathan, K.C. Wright, S.R. Muniz, M. Zelan, W.T. Hill, C.J. Lobb, K. Helmerson, W.D. Phillips, G.K. Campbell, Phys. Rev. Lett. **106**, 130401 (2011).
- [15] K.C. Wright, R.B. Blakestad, C.J. Lobb, W.D. Phillips, G.K. Campbell, Phys. Rev. Lett. **110**, 025302 (2013).
- [16] M. Cominotti, D. Rossini, M. Rizzi, F. Hekking, A. Minguzzi, arXiv:1310.0382
- [17] R. Kanamoto, H. Saito, M. Ueda, Phys. Rev. A **68**, 043619 (2003),
- [18] R. Kanamoto, L.D. Carr, M. Ueda, Phys. Rev. Lett. **100**, 060401 (2008)
- [19] R. Kanamoto, L.D. Carr, M. Ueda, Phys. Rev. A **79**, 063616 (2009)
- [20] A.Yu. Cherny, J.-S. Caux, J. Brand, Frontiers of Physics **7**, 54 (2012)
- [21] R. Ozeri, N. Katz, J. Steinhauer, N. Davidson, Rev. of Mod. Phys. **77**, 187 (2005).
- [22] L.D. Landau, J. Phys. (Moscow) **5**, 71 (1941).
- [23] V. Hakim, Phys. Rev. E **55**, 28352845 (1997)
- [24] M. Albert, T. Paul, N. Pavloff, P. Leboeuf, Phys. Rev. A **82**, 011602(R) (2010)
- [25] O. Morsch and M. Oberthaler, Rev. Mod. Phys. **78**, 179 (2006).
- [26] I. Bloch, J. Dalibard, and W. Zwerger, Rev. Mod. Phys. **80**, 885 (2008).
- [27] I. Brezinova, A.U.J. Lode, A.I. Streltsov, O.E. Alon, L.S. Cederbaum, J. Burgdorfer, Phys. Rev. A **86**, 013630 (2012)
- [28] A.I. Streltsov, K. Sakmann, O.E. Alon, L.S. Cederbaum, Phys. Rev. A **83**, 043604 (2011)
- [29] A. Polkovnikov, E. Altman, E. Demler, B. Halperin, M.D. Lukin, Phys. Rev. A **71**, 063613 (2005)
- [30] O. Fialko, M.-C. Delattre, J. Brand, A.R. Kolovsky, Phys. Rev. Lett. **108**, 250402 (2012)
- [31] J. C. Eilbeck, G. P. Tsironis, and S. K. Turitsyn, Phys. Scr. **52**, 386 (1995).
- [32] D. Hennig, H. Gabriel, M.F. Jorgensen, P.L. Christiansen, and C.B. Clausen, Phys. Rev. E **51**, 2870 (1995).
- [33] S. Flach and V. Fleurov, J. Phys.: Condens. Matter **9**, 7039 (1997).
- [34] K. Nemoto, C.A. Holmes, G.J. Milburn, and W.J. Munro, Phys. Rev. A **63**, 013604 (2000).
- [35] R. Franzosi and V. Penna, Phys. Rev. A **65**, 013601 (2002).
- [36] R. Franzosi, V. Penna, Phys. Rev. E **67**, 046227 (2003).
- [37] M. Hiller, T. Kottos, and T. Geisel, Phys. Rev. A **73**, 061604(R) (2006).
- [38] E. M. Graefe, H. J. Korsch, and D. Witthaut, Phys. Rev. A **73**, 013617 (2006).
- [39] J. D. Bodyfelt, M. Hiller, and T. Kottos, Europhys. Lett. **78**, 50003 (2007).
- [40] P. Buonsante, V. Penna, J. Phys. A **41**, 175301 (2008)
- [41] M. Hiller, T. Kottos, and T. Geisel, Phys. Rev. A **79**, 023621 (2009).
- [42] T.F. Viscondi, K. Furuya, J. Phys. A **44**, 175301 (2011)
- [43] P. Jason, M. Johansson, K. Kirr, Phys. Rev. E **86**, 016214 (2012)
- [44] H. Hennig, J. Dornigac, D.K. Campbell, Phys. Rev. A **82**, 053604 (2010) 1
- [45] Holger Hennig, Ragnar Fleischmann, Phys. Rev. A **87**, 033605 (2013)
- [46] T. Kottos, B. Shapiro, Phys. Rev. E **83**, 062103 (2011)
- [47] I. Tikhonenkov, A. Vardi, J.R. Anglin, D. Cohen, Phys. Rev. Lett. **110**, 050401 (2013).
- [48] Y. S. Kivshar and D. K. Campbell, Phys. Rev. E **48**, 3077 (1993).
- [49] B. Rumpf, Phys. Rev. E **70**, 016609 (2004).
- [50] A.M. Perelomov, Commun. Math. Phys. **26**, 222 (1972); arXiv:math-ph/0203002
- [51] M. Chuchem, K. Smith-Mannschott, M. Hiller, T. Kottos, A. Vardi, D. Cohen, Phys. Rev. A **82**, 053617 (2010).
- [52] C. Khripkov, D. Cohen, A. Vardi, J. Phys. A **46**, 165304 (2013).
- [53] C. Khripkov, D. Cohen, A. Vardi, Phys. Rev. E **87**, 012910 (2013).
- [54] E.J. Heller, in *Chaos and Quantum Physics*, edited by A. Voros and M.-J. Giannoni, Proceedings of the Les-Houches Summer School of Theoretical Physics, Session LII (North-Holland, Amsterdam, 1990).
- [55] L. Kaplan, E.J. Heller, Phys. Rev. E **59**, 6609 (1999).
- [56] P. Ghosh, F. Sols, Phys. Rev. A **77**, 033609 (2008)